Monthly Notices of the ROYAL ASTRONOMICAL SOCIETY

MNRAS **498,** 4943–4954 (2020) doi:10.1093/mnras/staa2731
Advance Access publication 2020 September 10

Are the Milky Way and Andromeda unusual? A comparison with Milky Way and Andromeda analogues

N. Boardman,[1]★ G. Zasowski,[1] J. A. Newman,[2] B. Andrews,[2] C. Fielder,[2] M. Bershady,[3,4,5] J. Brinkmann,[6] N. Drory,[7] D. Krishnarao,[3] R. R. Lane,[8,9] T. Mackereth,[10] K. Masters[11] and G. S. Stringfellow[12]

[1]*Department of Physics & Astronomy, University of Utah, Salt Lake City, UT 84112, USA*
[2]*Department of Physics & Astronomy and PITT PACC, University of Pittsburgh, Pittsburgh, PA 15260, USA*
[3]*Department of Astronomy, University of Wisconsin-Madison, 475N, Charter St, Madison WI 53703, USA*
[4]*South African Astronomical Observatory, PO Box 9, Observatory, 7935 Cape Town, South Africa*
[5]*Department of Astronomy, University of Cape Town, Private Bag X3, Rondebosch 7701, South Africa*
[6]*Apache Point Observatory, PO Box 59, Sunspot, NM 88349, USA*
[7]*McDonald Observatory, The University of Texas at Austin, 1 University Station, Austin, TX 78712, USA*
[8]*Pontificia Universidad Católica de Chile, Instituto de Astrofisica, Av. Vicuna Mackenna 4860, 782-0436 Macul, Santiago, Chile*
[9]*Instituto de Astronomía y Ciencias Planetarias, Universidad de Atacama, Copayapu 485, Copiapó, Chile*
[10]*School of Physics & Astronomy, University of Birmingham, Birmingham B15 2TT, UK*
[11]*Department of Physics and Astronomy, Haverford College, 370 Lancaster Ave, Haverford, PA 19041, USA*
[12]*Department of Astrophysical and Planetary Sciences, Center for Astrophysics and Space Astronomy, University of Colorado, 389 UCB, Boulder, CO 80309-0389, USA*

Accepted 2020 September 2. Received 2020 September 2; in original form 2020 May 16

ABSTRACT

Our Milky Way provides a unique test case for galaxy evolution models because of our privileged position within the Milky Way's disc. This position also complicates comparisons between the Milky Way and external galaxies, due to our inability to observe the Milky Way from an external point of view. Milky Way analogue galaxies offer us a chance to bridge this divide by providing the external perspective that we otherwise lack. However, overprecise definitions of 'analogue' yield little-to-no galaxies, so it is vital to understand which selection criteria produce the most meaningful analogue samples. To address this, we compare the properties of complementary samples of Milky Way analogues selected using different criteria. We find the Milky Way to be within 1σ of its analogues in terms of star formation rate and bulge-to-total ratio in most cases, but we find larger offsets between the Milky Way and its analogues in terms of disc scale length; this suggests that scale length must be included in analogue selections in addition to other criteria if the most accurate analogues are to be selected. We also apply our methodology to the neighbouring Andromeda galaxy. We find analogues selected on the basis of strong morphological features to display much higher star formation rates than Andromeda, and we also find analogues selected on Andromeda's star formation rate to overpredict Andromeda's bulge extent. This suggests both structure and star formation rate should be considered when selecting the most stringent Andromeda analogues.

Key words: galaxies: general – galaxies: spiral – galaxies: statistics – galaxies: stellar content – galaxies: structure – Galaxy: general.

1 INTRODUCTION

The question of how galaxies form and evolve remains a problem of significant interest in extragalactic astrophysics. The last two decades have seen a major progress on this topic because of the census of local Universe galaxies undertaken by the Sloan Digital Sky Survey (SDSS; York et al. 2000). SDSS data conclusively demonstrated a bimodality in terms of both galaxies' integrated colors (Strateva et al. 2001) and integrated magnitudes (Baldry et al. 2004), with the majority of galaxies being either star-forming 'blue cloud' galaxies or quiescent 'red-sequence' galaxies. At the same time, a minority of galaxies can be seen to occupy the intermediate 'green valley' when plotted on colour–magnitude diagrams. It is commonly accepted that the green valley is occupied by galaxies in the process of transitioning from star-forming to quiescent. However, a large number of precise evolution pathways are needed to fully explain the range of observed galaxy properties such as integrated colour, star formation rate (SFR), and morphology (e.g. Bell et al. 2004; Faber et al. 2007; Schawinski et al. 2014; Smethurst et al. 2015).

Our own Milky Way (MW) remains a key source of insight into both the structures of galaxies and the physics of galaxy evolution on small scales. Traditionally, the MW has been understood to contain both a younger 'thin disc' and an older alpha-enhanced 'thick

★ E-mail: nick.boardman@astro.utah.edu

disc' (Yoshii 1982; Gilmore & Reid 1983; Chiappini, Matteucci & Gratton 1997; Bensby, Feltzing & Lundström 2003; Haywood et al. 2013; Xiang et al. 2017; Wu et al. 2019), which produces an observed bimodality in alpha abundance ratios at intermediate MW stellar metallicities (e.g. Fuhrmann 1998, 2011; Anders et al. 2014; Mikolaitis et al. 2014; Nidever et al. 2014; Recio-Blanco et al. 2014; Hayden et al. 2015); such a bimodality is observed in both the MW's disc (e.g. Hayden et al. 2015) and bulge (Queiroz et al. 2019; Rojas-Arriagada et al. 2019). The MW's inner region is dominated by a cylindrical-rotating boxy-peanut 'pseudo-bulge' (e.g. Dwek et al. 1995; McWilliam & Zoccali 2010) along with a stellar bar (e.g. Hammersley et al. 1994; Weiland et al. 1994; Wegg & Gerhard 2013). In addition, the MW may also contain a small 'classical' bulge component made up of old stars (e.g. Dékány et al. 2013; Barbuy, Chiappini & Gerhard 2018).

The last decade has proven particularly fruitful in regards to our understanding of the MW, with a number of spectroscopic surveys observing stars over large regions of the MW's stellar disc. These surveys include RAVE (Steinmetz et al. 2006), LEGUE (Deng et al. 2012), LAMOST (Cui et al. 2012), the *Gaia*–ESO survey (Gilmore et al. 2012), GALAH (De Silva et al. 2015), and APOGEE (Majewski et al. 2017). Such data sets have challenged the traditional two-population view of the MW's stars, with the MW instead appearing to consist of a broad continuum of chemo-dynamical stellar subpopulations (e.g. Bovy, Rix & Hogg 2012; Mackereth et al. 2017; Buder et al. 2019). Furthermore, it has become clear that the geometrical thin and thick discs of the MW are *not* the same structures as the chemical thin and thick discs (e.g. Minchev et al. 2015; Martig et al. 2016).

However, the MW's position within the galactic population remains poorly understood, which complicates the interpretation of MW results in the wider extragalactic context. This situation results from our position within the MW's disc, from which large regions of the MW remain difficult to observe. Dust extinction preferentially reddens stars away from the solar region, limiting the number of stars that can be observed particularly at UV and optical wavelengths (e.g. Schlegel, Finkbeiner & Davis 1998; Schlafly & Finkbeiner 2011; Queiroz et al. 2019); this especially complicates the analysis of stars beyond the central stellar bulge and bar. It is therefore difficult to determine integrated quantities for the MW such as optical colour (e.g. Mutch, Croton & Poole 2011), which can be straightforwardly calculated for nearby galaxies.

It thus remains unclear how common the MW's properties are within the wider galaxy population. A particular open question concerns the size of the MW's disc component, which has repeatedly been argued to be comparatively low (e.g. Bland-Hawthorn & Gerhard 2016; Licquia, Newman & Bershady 2016). The MW disc appears to be more compact than the majority of galaxies of MW-like mass (e.g. Bovy & Rix 2013; Licquia & Newman 2016, hereafter LN16) and appears to be deficient by around 1σ with respect to the MW's circular velocity (Hammer et al. 2007), whereas the scale length of M31 appears far more usual (Hammer et al. 2007). The MW displays properties in good consistency with other galaxies once its disc's compactness is taken into account, meanwhile (Bovy & Rix 2013; Boardman et al. 2020).

Milky Way Analogues (MWAs) provide an ideal opportunity to bridge the gap between Galactic and extragalactic observations. MWAs allow one to estimate global properties of the MW that cannot be easily or directly estimated for the MW, and have enabled tight estimates of the MW's magnitude and colour (Licquia, Newman & Brinchmann 2015). MWAs also allow comparison of the MW to its immediate peers (e.g. Fraser-McKelvie, Merrifield & Aragón-Salamanca 2019; Boardman et al. 2020; Krishnarao et al. 2020). Thus, MWAs are a powerful tool for better understanding the MW in the extragalactic context.

However, there is no one definition for what makes a galaxy a MWA, and overly strict definitions of 'analogue' can produce negligible or even flat-out non-existent samples of MWA galaxies. Fraser-McKelvie et al. (2019), for instance, find just 176 MWAs from selecting on stellar mass, bulge-to-total ratio (B/T) and morphology. Boardman et al. (2020), meanwhile, find not a single MWA in the SDSS-IV (Blanton et al. 2017) MaNGA survey (Bundy et al. 2015) when attempting to select on a combination of stellar mass (M_*), SFR, B/T, and disc scale length (R_d). It is thus critical to assess the impact of different selection criteria, in order to understand how to best select constraining samples of MWAs.

M31 analogues, hereafter M31As, can provide us with additional insight. M31As allow us to assess Andromeda's position amongst its peers in a similar manner to what MWAs enable for the MW. The MW and M31 are the two nearest massive disc galaxies to us, and can both be studied in much greater depth than other such galaxies; thus, it is crucial to understand how both the MW and M31 relate to the wider extragalactic population.

We experiment here with a number of complementary selection criteria, aimed at selecting various samples of 'analogues' and then comparing their ranges of properties to our knowledge of the MW. We perform an equivalent analysis on M31A galaxies, selecting M31As through multiple means and then comparing with M31.

This paper is organized as follows. In Section 2, we describe the methodology behind our various sample selections, and then in Section 3 we present our results in terms of the samples' properties and their comparison to the MW and to M31. We discuss our findings and conclude in Section 4.

2 SAMPLE AND DATA

In Section 2.1, we discuss the acquisition of all parameters being considered in our selections as well as in our analysis. We discuss our MWA selections in Section 2.2 and our M31A selections in Section 2.3.

2.1 Source catalogues

We obtain stellar masses, SFRs, B/T ratios, disc scale lengths, multi-band magnitudes, redshifts, and quantitative galaxy morphologies by cross-referencing a number of published catalogues. We consider in our subsequent analysis only galaxies that are present in all catalogues.

We obtain total stellar masses and current global SFRs from the Galaxy Evolution Explorer (*GALEX*)–SDSS–WISE Legacy catalogue (GSWLC; Salim et al. 2016), employing the GSWLC-2X catalogue (Salim, Boquien & Lee 2018). GSWLC-2X contains stellar masses and SFRs for 659229 galaxies, selected by cross-referencing the spectroscopic SDSS Data Release 10 (DR10; Ahn et al. 2014) sample with the ultraviolet *GALEX* (Martin et al. 2005) sample. Masses and SFRs are derived through spectral energy distribution fits performed using the Code Investigating GALaxy Emission (Noll et al. 2009; Boquien et al. 2019), which uses WISE (Wright et al. 2010) IR luminosity as a constraint on UV-optical fits to combined *GALEX*–SDSS photometry. The GSWLC masses and SFRs assume a Chabrier (2003) initial mass function (IMF); we converted these to a Kroupa (2001) IMF by multiplying by a factor of 1.06 (Elbaz et al. 2007; Salim et al. 2007; Zahid et al. 2012).

We obtain light-weighted *r*-band B/T and R_d values from the catalogue of Simard et al. (2011), who perform bulge–disc decompositions of 1 123 718 galaxies from the SDSS Data Release 7 (DR7;

Table 1. MWA sample definitions, in addition to $M_* = 4.6 - 7.2 \times 10^{10}\,\mathrm{M}_\odot$, $z \leq 0.06$, $P_{pS} \leq 0.32$ and $b/a \geq 0.6$.

Analogue sample	SFR ($\mathrm{M}_\odot\ \mathrm{yr}^{-1}$)	B/T	R_d (kpc)	Galaxy Zoo vote fraction
MW star formation analogues	1.46–1.84	–	–	–
MW bulge analogues	–	0.13–0.19	–	–
MW scale analogues	–	–	2.51–2.93	–
MW morphological analogues	–	–	–	spiral > 0.8, bar > 0.8, $N_{\mathrm{bar,\ spiral}} \geq 20$ smooth ≤ 0.57, edgeon ≤ 0.285

Abazajian et al. 2009). Specifically, we employed the two-component bulge+disc fits from that paper in which the bulge Sérsic index n_b was treated as a free parameter. Simard et al. (2011) perform their fits simultaneously to *g*-band and *r*-band SDSS galaxy photometry; structural parameters including n_b and R_d are fixed to be identical in both bands, whereas the amplitude of individual components (and hence B/T) are allowed to vary between bands. We also obtain from this catalogue the P_{pS} ('probability of pure Sérsic') parameter for each galaxy. P_{pS} denotes the *F*-test probability of a bulge+disc model *not* being required to fit a given galaxy, as opposed to a pure Sérsic model, and parametrizes the goodness-of-fit improvement achieved by fitting a bulge+disc component over a single Sérsic component.

We obtain redshifts and absolute magnitudes from version 1.0.1 of the NASA–Sloan Atlas[1] (NSA) catalogue (Blanton et al. 2011), which re-reduces the data in SDSS Data Release 8 (DR8; Aihara et al. 2011). The NSA absolute magnitudes are drawn from a combination of *GALEX* and SDSS photometry, and are provided over seven bands (FNugriz) overall; we use the elliptical Petrosian set of values throughout our analysis. For redshifts, we use values obtained from the distance estimates of Willick et al. (1997).

Finally, we obtain measurements of galaxy morphologies from the Galaxy Zoo 2 catalogue (GZ2; Willett et al. 2013), employing user-weighted vote fractions along with the redshift-debiased fractions described in Hart et al. (2016). We obtained information on the presence of bar and spiral features along with information concerning the galaxies' inclinations. The Galaxy Zoo vote-based method allows quantitative measures of morphology as well as providing quantitative confidence levels in those morphologies, and has repeatedly been shown to be an excellent means of detecting spiral arms and bars (e.g. Hart et al. 2017; Kruk et al. 2018). The specific parameters we extracted from the catalogue were 't01_smooth_or_features_a01_smooth_weighted_fraction', 't02_edgeon_a04_yes_weighted_fraction', 't03_bar_a06_bar_debiased', 't04_spiral_a08_spiral_debiased', 't03_bar_a06_bar_count' and 't04_spiral_a08_spiral_count'; for the remainder of this paper, we will refer to these parameters respectively as *smooth*, *edgeon*, *bar*, *spiral*, N_bar, and N_spiral. We will also refer to a parameter $N_{\mathrm{bar,\ spiral}}$, describing the lower value out of N_bar and N_spiral for a given galaxy.

We obtain a total of 149 585 galaxies from this cross-referencing procedure. Following Simard et al. (2011), we discount all galaxies for which $P_{pS} > 0.32$, as such galaxies are less likely to be true bulge+disc systems and so are more likely to yield spurious bulge–disc decompositions; this yields 82 724 galaxies. We then remove all galaxies with elliptical Petrosian axis ratios (b/a) below 0.6, to avoid considering discy galaxies with edge-on viewing angles and so strong internal dust extinction (e.g. Licquia et al. 2015), leaving 62 735 galaxies; we discuss this cut further in the following subsection.

[1] http://www.nsatlas.com

We further remove 1337 galaxies for which $R_\mathrm{d} < 1$ and $B/T > 0.8$, in order to eliminate galaxies with unreliable bulge+disc fits that were not eliminated by the previous cut. This produces a final parent sample of 61 398 galaxies, from which we select MWA and M31A samples as described in the following subsections.

We employ *volume-limited* analogue samples throughout our analysis. Essentially, we wish to ensure that we do not miss fainter MWAs/M31As due to the magnitude limits of employed galaxy catalogues, allowing unbiased comparisons with the MW and M31. We achieve this by restricting analogue samples to a given maximum redshift, as described in the next two subsections for MWAs and M31As, respectively.

2.2 Milky Way analogue sample selections

We select a series of MWA samples based on our knowledge of the MW. Each sample is based on a different definition of 'analogue', as described in the remainder of this section and summarized in Table 1.

Our MWA selections are largely based on the MW parameter values reported in Licquia & Newman (2015; hereafter LN15) and LN16. These two works combine a wide variety of literature measurements in order to obtain constraints on the MW's M_*, SFR, B/T, and R_d values. LN15 determine the MW SFR by performing a Heiarchical Bayesian analysis on a range of previous SFR measurements retrieved from table 1 of Chomiuk & Povich (2011). LN16 similarly obtain an MW R_d value by combining numerous individual measurements (e.g. Kent, Dame & Fazio 1991; Ruelas-Mayorga 1991; Chen et al. 1999; Benjamin et al. 2005; Chang, Ko & Peng 2011; Mao et al. 2015), with the value effectively being an estimate for the MW's thin disc. M_* and B/T values are determined by combining stellar bulge and/or bar mass values from the literature (e.g. Kent 1992; Dwek et al. 1995; Widrow, Pym & Dubinski 2008) and then using these in conjuction with Monte Carlo simulations of an exponential disc model based on Bovy & Rix (2013). LN15 employ an R_d value of 2.15 ± 0.14 for this process, from Bovy & Rix (2013), whereas LN16 employ their own R_d estimate.

The galactic parameters we consider are likely to vary over a variety of different time-scales. In particular, the SFR is expected to fluctuate relatively rapidly over a galaxy's lifetime, whereas a galaxy's mass and stucture will change far more gradually. In general, the key assumption behind MWA selections is that the MW *should not be unusual* amongst a sample of its chosen analogues (e.g. Licquia et al. 2015; Boardman et al. 2020), regardless of the specific parameters employed in selections. Thus, it is worthwhile to consider both long-lived and shorter-lived parameters when selecting MWA samples.

We select 'star formation MWAs' (hereafter 'SF MWAs') based on stellar masses and SFRs. This is a natural MWA definition, as both parameters are known to be strongly correlated with galaxies' global

photometric properties (Licquia et al. 2015). We select galaxies with stellar masses between $4.6 \times 10^{10}\,M_\odot$ and $7.2 \times 10^{10}\,M_\odot$, based on the 1σ confidence intervals reported in LN15. We then further limit the sample to those galaxies with SFR values between 1.46 and 1.84 $M_\odot\,yr^{-1}$, based on the 1σ interval found in LN16.

We select 'bulge MWAs' by cutting on stellar masses and B/Ts. This is another natural choice for performing MWA selections, due to the known connection between the growth of a galaxy's bulge with a galaxy's particular evolution history (e.g. Cappellari 2016; Belfiore et al. 2017; Saha & Cortesi 2018). We perform the same mass cut as before, and we select galaxies with B/T values between 0.13 and 0.19 based on the LN16 1σ intervals.

We select 'scale MWAs' based on stellar mass and on exponential disc scale length. The MW scale length has repeatedly been suggested to be atypically short for the MW's stellar mass; thus, scale length is potentially important for understanding the MW's place in the wider extragalactic context (Boardman et al. 2020). We use the same mass cut as before, and we further cut the sample to include only galaxies with R_d values between 2.51 and 2.93 kpc; this is based on the 1σ intervals reported in LN16 from optical data only, as opposed to the intervals from IR or optical+IR data.

Licquia et al. (2016) discuss at length the applicability of the MW scale length for comparing with external galaxy measurements in their section 5.2.1; we provide a brief summary here, and direct the interested reader to that paper for a more complete discussion. MW disc scale length calculations are typically carried out via star-count analyses, which differs significantly from the photometric methods employed for other galaxies. On the other hand, the ratio between the MW's IR and visible scale lengths appears similar to that measured for external galaxies, and MW dynamical scale length measurements are consistent with measurements made through other means (LN16); thus, the MW scale lengths reported in the literature appear robust for our purposes.

Lastly, we select a sample of 'morphological MWAs', defined as those galaxies with masses in the 1σ MW range that also possess bar and spiral features. The presence of a bar in particular is likely important in understanding a given galaxy's properties (e.g. Krishnarao et al. 2020), making it worthwhile to explore barred spiral analogues separately from the previously defined samples. We largely follow table 3 of Willett et al. (2013) in performing this selection: we restrict to galaxies satisfying *smooth* ≤ 0.57, *edgeon* ≤ 0.285, and $N_{\rm bar,\,spiral} \geq 20$. For conservative sample selections, Willett et al. (2013) further suggest using minimum vote thresholds of 0.8 for selecting on morphological features, and we employ those thresholds on the *bar* and *spiral* vote fractions. We show some examples morphological MWAs in Fig. 1.

Measured bulge MWA properties are relatively sensitive to viewing angle, given the status of bulge MWAs as disc-dominated systems. In Fig. 2, we the SFR and R_d values of bulge MWAs in bins of b/a, in the case where no b/a cut is applied to the parent sample. We find a small but non-negligible drop in SFR at b/a < 0.6 along with a significant increase in R_d at b/a values below 0.4. Thus, a b/a cut is necessary to avoid biases in the properties of sample galaxies.

We restrict all four MWA samples to galaxies of redshifts $z \leq 0.06$, in order to ensure that the samples are volume limited. In Fig. 3, we show the magnitudes and redshifts of the bulge MWA sample along with all galaxies that satisfy the MW mass cut. By limiting to $z \leq 0.06$, we obtain volume-limited samples as desired; the same situation occurs for the other three MWA samples.

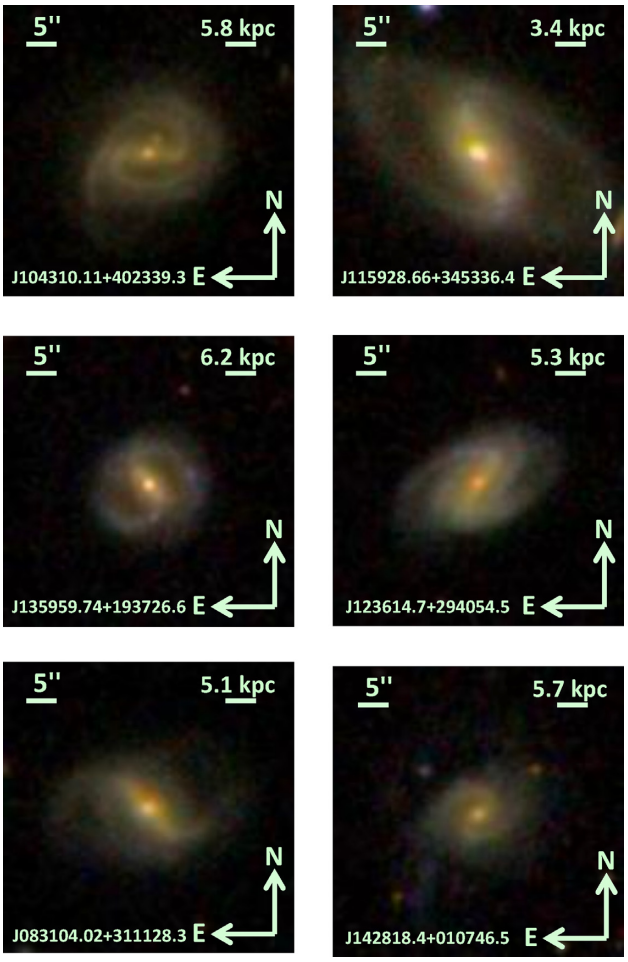

Figure 1. Example morphological MWAs, selected on mass and on Galaxy Zoo morphology votes as discussed in the text.

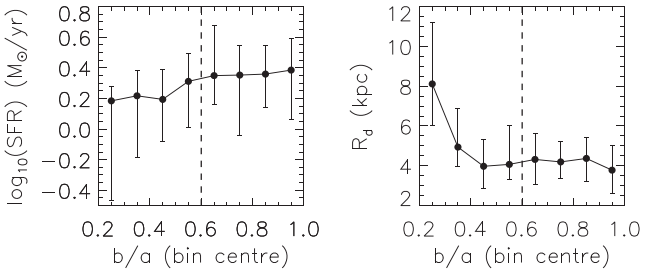

Figure 2. Medians and 1σ intervals of SFR (left-hand panel) and R_d (right-hand panel) for bulge MWAs binned by b/a, in the case where no b/a cut is applied to the parent sample. The dashed lines mark where b/a =0.6, below which galaxies are *not* included in the parent sample and so not included in any subsequent analysis.

In Fig. 4, we show the size of the selected MWA samples in the form of a Venn diagram, along with the numbers of galaxies satisfying different combinations of parameter cuts. We find that the number of identified MWAs becomes vanishingly small as the number of criteria is increased, with not one MWA satisfying all of the cuts. This problem of dimensionality was previously highlighted in Fraser-McKelvie et al. (2019), and demonstrates the need to employ just a few selection criteria when large MWA samples are required.

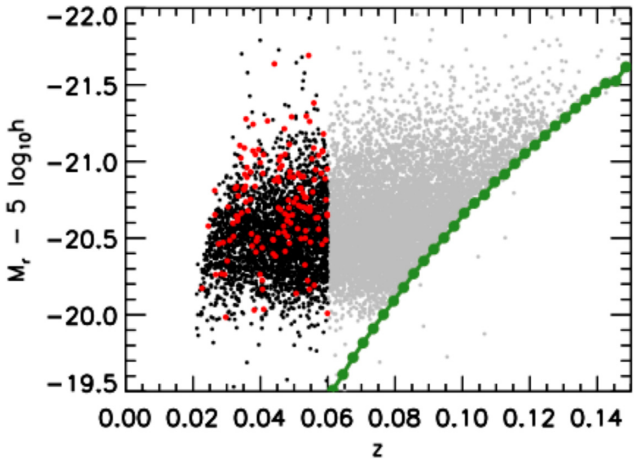

Figure 3. Plot of *r*-band absolute magnitude versus redshift for the bulge MWA sample (the red points), along with all galaxies satisfying the MW mass cut inside (the black points) and outside (the grey points) the volume-limited redshift region. The green points show the 99th percentile absolute magnitude of the parent sample as a function of redshift.

Many additional possible 'analogue' definitions exist beyond the ones we consider here. The nearby NGC 891, for instance, is often considered an MWA on the basis of morphology and rotational velocity (e.g. Mouhcine, Ibata & Rejkuba 2010; Hughes et al. 2014). Kormendy & Bender (2019) argue NGC 4565 and NGC 5746 to be analogues on the basis of their morphology, and in particular on the presence of boxy pseudo-bulges. A search for boxy bulge structures is possible with SDSS imaging (Yoshino & Yamauchi 2015) but would require edge-on samples, and so conflicts with the requirements of the other analogue samples in this work. An analogue sample based on rotational velocities is more feasible but of questionable additional value, particularly in light of the stellar mass Tully–Fisher relation (TFR; Tully & Fisher 1977; Mocz et al. 2012; Licquia et al. 2016). It should also be noted that in Licquia et al. (2016), the quoted uncertainty in the MW rotational velocity is larger than the uncertainty in the stellar mass, relative to the scatter in the stellar mass TFR itself.

2.3 M31 analogue sample selections

As with the MW, a range of calculations of key M31 properties have been performed over the years. M31 is known to be more massive than the MW, and has consistently been measured to possess a significantly larger disc scale length (e.g. Hammer et al. 2007). In addition, M31 is generally agreed to possess a lower current SFR than the MW (e.g. Yin et al. 2009, and references therein). Our M31 sample selections are designed to capture this behaviour, while allowing for the spread in reported M31 measurements. We summarize our M31A selections in Table 2, and we explain our selections over the remainder of this subsection.

First, we restrict all M31A selections to galaxies with masses between $9.9 \times 10^{10}\,M_\odot$ and $1.09 \times 10^{11}\,M_\odot$. We obtained this range from Mutch et al. (2011), who computed it from from the semi-analytic mass modelling of Geehan et al. (2006) and other compiled literature values (e.g. Barmby et al. 2006; Hammer et al. 2007).

We select a sample of 'star formation M31As' (hereafter 'SF M31As') using the M31 SFRs calculated over 10 Myr by Kang, Bianchi & Rey (2009), as presented in their table 3 based on combined UV and IR photometry. Taking for boundaries the values calculated with stellar model grids with subsolar ($Z = 0.008$) and supersolar ($Z = 0.05$) metallicities, respectively, we obtain an SFR range of 0.41–0.83 $M_\odot\,yr^{-1}$. This is broadly consistent with the range of values reported in past literature (see e.g. table 1 of Yin et al. 2009). Where necessary, we assume a mid-point M31 SFR of 0.46 $M_\odot\,yr^{-1}$, calculated with solar-metallicity ($Z = 0.02$) model grids.

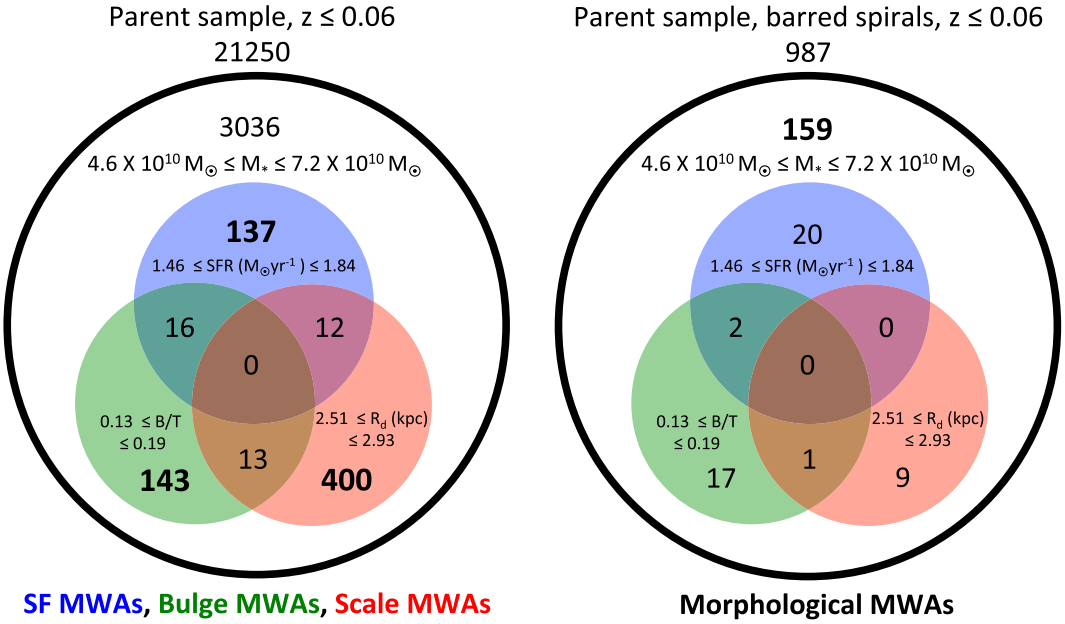

Figure 4. Venn diagrams showing the numbers of galaxies satisfying the MWA cuts discussed in the text. Barred spirals are defined by Galaxy Zoo vote fractions as described in the text for the morphological MWAs.

Table 2. M31A sample definitions, in addition to $M_* = 9.9 \times 10^{10} - 1.09 \times 10^{11}$ M$_\odot$, $z \leq 0.09$, $P_{pS} \leq 0.32$, and $b/a \geq 0.6$.

Analogue sample	SFR (M$_\odot$ yr^{-1})	B/T	R_d (kpc)	Galaxy Zoo vote fraction
M31 star formation analogues	0.41–0.83	–	–	–
M31 bulge analogues	–	0.24–0.42	–	–
M31 scale analogues	–	–	4.8–5.8	–
M31 morphological analogues	–	–	–	spiral > 0.8, bar < 0.2, $N_{spiral} \geq 20$ smooth ≤ 0.57, edgeon ≤ 0.285

We select 'bulge M31As' by considering all results contained within table 5 of Tamm et al. (2012), along with the results of Barmby et al. (2006) and Courteau et al. (2011). We take the mean and standard deviation of the resulting B/T values, obtaining a value of $B/T_{M31} = 0.33 \pm 0.09$; we use this value to define our M31 structural analogue sample, employing a cut-off $B/T = 0.24-0.42$.

We select a sample of 'scale M31As' using the 5.3 ± 0.5 kpc M31 disc scale length reported by Courteau et al. (2011) from infrared *Spitzer*/IRAC imaging. This is slightly lower than the majority of photometric measurements, as can be seen in Hammer et al. (2007) and Yin et al. (2009) along with references therein; Hammer et al. (2007) use a value of 5.8 ± 0.4 kpc to represent the range of reported photometric values, for instance. However, the Courteau et al. (2011) value is more analogous to the (effectively mass-weighted) value we employ for the MW and less sensitive to dust extinction effects than measurements made in bluer bands. In addition, the choice between the M31 R_d values of Courteau et al. (2011) and Hammer et al. (2007) matters little in practice, as they are both consistent with M31 having a scale length that is reasonably standard for a galaxy of its mass (e.g. Fathi et al. 2010; Wu 2018).

Finally, we select a sample of 'morphological M31As' based on GZ2 vote fractions. M31 is known to contain a stellar bar (e.g. Beaton et al. 2007), but visually appears as an unbarred spiral galaxy (e.g. Sandage & Tammann 1981); thus, we select for the presence of spiral features along with the apparent *absence* of bar features. As for the MWAs, we restrict to galaxies satisfying *smooth* ≤ 0.57, *edgeon* ≤ 0.285. We then use selection thresholds of spiral > 0.8 and bar < 0.2, along with requiring $N_{spiral} \geq 20$; we impose no requirement on N_{bar} in this case, as low *bar* values typically correspond to low N_{bar} numbers. We present some example morphological M31As in Fig. 5.

We restrict all M31A samples to galaxies with redshifts $z \leq 0.09$ to ensure volume limiting; we are able to use a higher maximum redshift in this case due to the brighter magnitudes displayed by the M31As. We present the ranges of redshifts and magnitudes of the bulge M31A samples in Fig. 6, wherein we show that our adopted redshift cut leads to a volume-limited sample as desired; the same situation is seen in all M31A samples. We present Venn diagrams detailing the M31A sample sizes in Fig. 7.

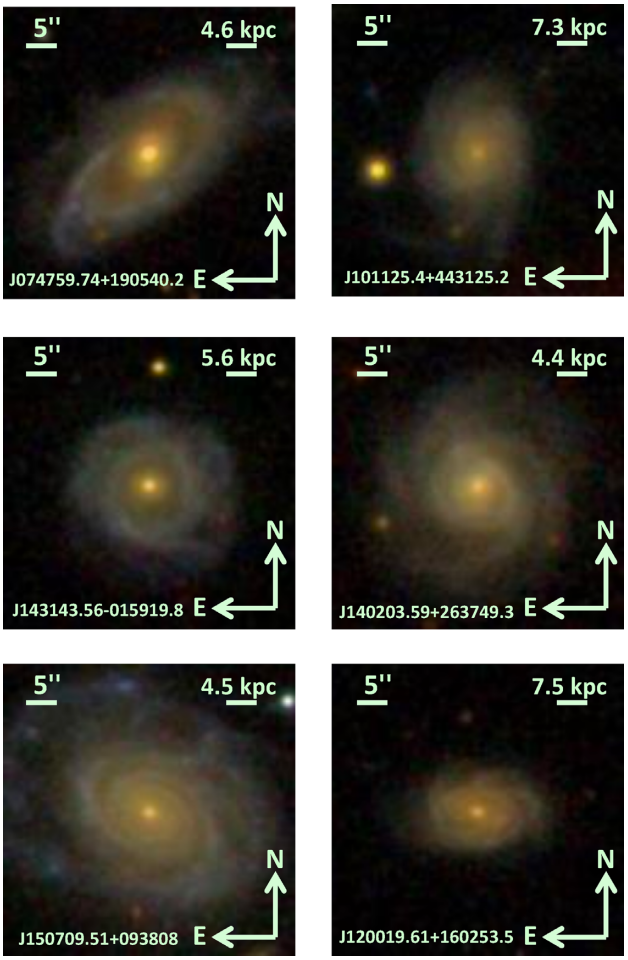

Figure 5. Example morphological M31As, selected as discussed in the text.

3 RESULTS

3.1 MWA results

In the left-hand panel of Fig. 8, we show the B/T and R_d distributions of the SF MWAs as a 2D histogram, along with the MW value and contours of properties for all galaxies that satisfy the MW mass cut. We find the MW to lie within 1σ of the B/T values calculated for SF analogues, though we note that the range of B/T values amongst SF MWAs is wide. The MW is somewhat of an outlier in terms of scale length, but remains within the 2σ region.

We plot the SFR and R_d values of the bulge MWAs in the middle panel of Fig. 8, in which we find the adopted MW SFR to lie well within 1σ of the bulge MWAs. We find the MW disc scale length to again be low compared to the majority of bulge MWAs, though still within 2σ of this sample.

The right-hand panel of Fig. 8 presents the properties of the scale MWAs in terms of SFR and B/T, following the same format as the preceding two panels. We see the expected star-forming/quiescent galaxy dichotomy in the mass-selected sample, with a discy star-forming component along with a quiescent and more bulgey component; we find this dichotomy to be maintained amongst the scale analogues, albeit weighted more heavily towards the quiescent component. We also find amongst the discy scale analogues, the MW *does not appear to be unusual*, with both an SFR and B/T in good consistency with the behaviour of the discy scale analogues.

We present in Fig. 9 1D histograms of properties of the morphological MWAs in terms of SFR, B/T, and R_d in turn. We caution though that the B/T and R_d values are specifically calculated from

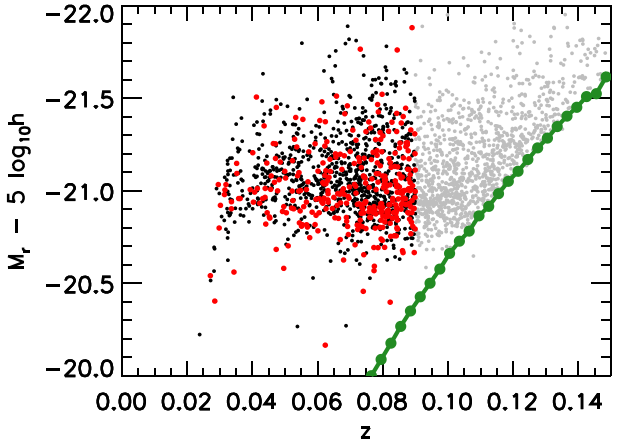

Figure 6. Plot of *r*-band absolute magnitude versus redshift for the bulge M31A sample (the red points), along with all galaxies satisfying the M31 mass cut inside (the black points) and outside (the grey points) the volume-limited redshift region. The green points show the 99th percentile absolute magnitude of the parent sample as a function of redshift.

two-component photometric fits, which will not fully capture the photometry of barred galaxies and can significantly overestimate barred galaxies' B/Ts (Laurikainen, Salo & Buta 2005; Laurikainen et al. 2006; Kruk et al. 2018); thus, we include B/T and $R_{\rm d}$ values purely for completeness in this case. In terms of SFR, we find the MW to well within 1σ of the morphological MWA sample.

Overall, the SF, bulge, and morphological MWAs are broadly consistent in their range of properties, with all three favouring the selection of disc-dominated star-forming galaxies. It is apparent that MWA samples do *not* accurately predict the MW's short scale length unless the scale length is specifically selected on, and it is also apparent that the scale MWA sample is not particularly constraining in itself. At the same time, the MW appears to not be the least bit unusual amongst the star-forming galaxies within the scale MWA sample. From these findings, we argue that scale length should be considered *in addition* to other parameters in order to select the most stringent MWA galaxies.

3.2 M31A results

We plot the SF M31A sample in terms of B/T and $R_{\rm d}$ in the left-hand panel of Fig. 10, with our adopted M31 values shown on the same figure along with contours of all galaxies satisfying our M31 mass cut. We find M31's scale length to be in excellent agreement with the SF M31As. However, we find the SF M31As to overpredict the B/T to an extent, with M31's B/T offset low by approximately 1σ.

We present in the middle panel of Fig. 10 the bulge M31A sample in terms of SFR and $R_{\rm d}$. We find the M31 SFR to be slightly low amongst the bulge M31As, though still well within 1σ of this sample's range. We also find the scale lengths of the bulge M31As to agree excellently with that of M31.

We present the SFR and B/T distributions of the scale M31A sample in the right-hand panel of Fig. 10. We find M31 to within 1σ in terms of both properties when the properties are considered individually, but it is clear that M31's SFR is somewhat lower than is typical for scale M31As in M31's likely B/T range.

Lastly, we present the properties of the morphological M31As in Fig. 11. We find our adopted central M31 SFR to be offset low by more than 2σ in this case, while finding M31's B/T and $R_{\rm d}$ to both not be the least bit unusual amongst the morphological M31As.

To summarize, we find the scale length of M31 to agree excellently with those of the M31A samples, but we find the SFR of M31 to be somewhat low. Although M31's SFR is in reasonable consistency with the bulge and scale M31A samples, it is significantly offset from the morphological M31As. In addition, M31's low SFR leads the SF M31A sample to overpredict M31's B/T by around 1σ. From this, we advocate including mass and B/T in selection criteria for targeting the closest M31As, with M31's low SFR also important to keep in mind.

4 DISCUSSION AND CONCLUSIONS

In this paper, we have explored the properties of various galaxy samples selected as 'MWAs' or 'Andromeda Analogues' using various selection criteria. We compared the properties of both the MW and M31 to their respective analogues, with the aim of understanding how to best select constraining 'analogue' samples.

Critically, the MWA samples do *not* accurately predict the short disc scale length of the MW unless the scale length is included in the selection criteria. Although a few reported MW $R_{\rm d}$ values are highly consistent with our non-scale MWA samples (e.g. Yamagata & Yoshii 1992; Benjamin et al. 2005; Chang et al. 2011; Grady, Belokurov & Evans 2020), the vast majority of measurements are less so (e.g. Kent et al. 1991; Ruelas-Mayorga 1991; Chen et al. 1999; Bovy & Rix 2013; Mao et al. 2015; Li et al. 2018b). The scale length of the MW disc is therefore important to consider if one wishes to select the most similar MWA galaxies.

It should be noted that the MW's scale length is *not unduly unusual* amongst those of the MW's direct peers, with the MW scale length remaining within 2σ of the SF and bulge MWAs. In turn, the MW appears not the least bit unusual amongst star-forming scale MWAs, with the MW's SFR and B/T values both well within the scale MWA sample's range. Thus, while the MW is indeed an outlier in terms of $R_{\rm d}$, it is not an outlier to the extent of requiring a unique explanation.

Aside from the MW's short scale length, the MW is likewise not unusual amongst the other MWA samples considered. In terms of B/T, the MW falls within the 1σ range displayed by the SF MWAs; likewise, the SFR of the MW falls well within 1σ of the SFR range of the bulge MWAs. We also find the MW SFR to be well within 1σ of the morphological MWAs. Overall, we find the MW to be a relatively typical galaxy aside from its short disc scale length, consistent with previous work (e.g. Hammer et al. 2007; Bovy & Rix 2013; Licquia et al. 2016).

In contrast to the MW, we find M31's SFR to be overpredicted to various extents in all non-SF M31A samples. In turn, the SF M31As overpredict M31's B/T. Thus, we argue that the combination of a low SFR and relatively low B/T are important in selecting the closest M31A galaxies. Our results here are in good consistency with the work of Mutch et al. (2011), who argue M31's properties to be consistent with galaxies on the green valley region of the colour–magnitude diagram. Compared to the MW, we also find M31's disc scale length to be in much greater consistency with its respective analogue samples, which is likewise consistent with previous work (e.g. Hammer et al. 2007).

Similar results can be expected if one parametrizes galaxy mass with $V_{\rm rot}$ instead of stellar mass, due to the existence of the stellar mass TFR. We confirmed this by cross-matching our parent sample with the ALFALFA extragalactic H I source catalogue (Haynes et al. 2018), converting velocity widths to $V_{\rm rot}$ using inclinations obtained from Simard et al. (2011). We adopted MW and M31 $V_{\rm rot}$ values of 220 ± 22 km s^{-1} (Kerr & Lynden-Bell 1986) and 226 ± 29 km s^{-1} (Carignan et al. 2006), respectively, where we have

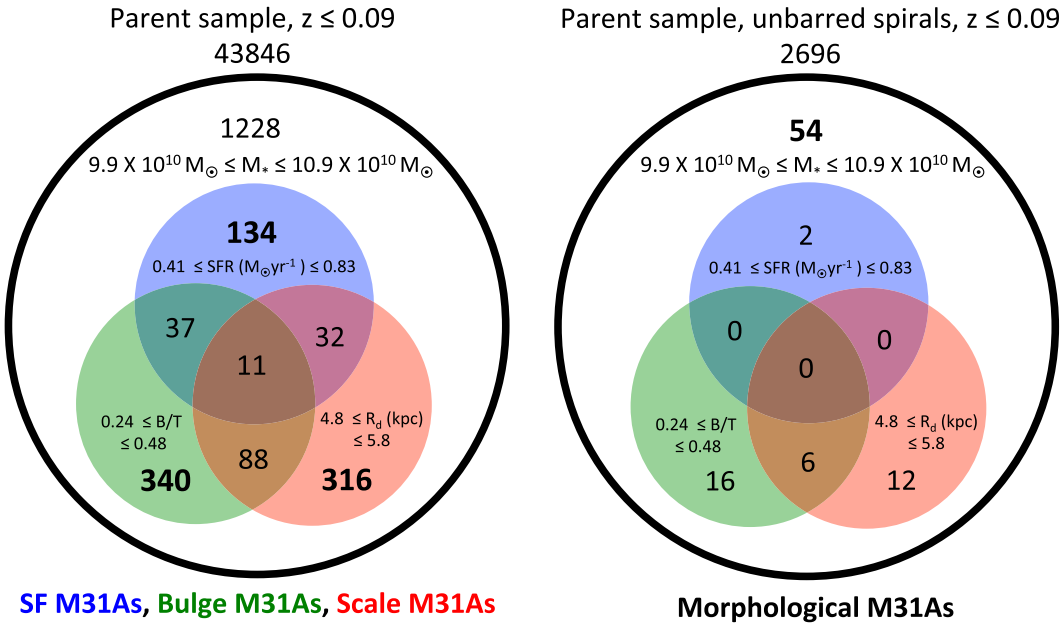

Figure 7. Venn diagrams showing the numbers of galaxies satisfying the M31A cuts discussed in the text. Unbarred spirals are defined by Galaxy Zoo vote fractions as described in the text for the morphological M31As.

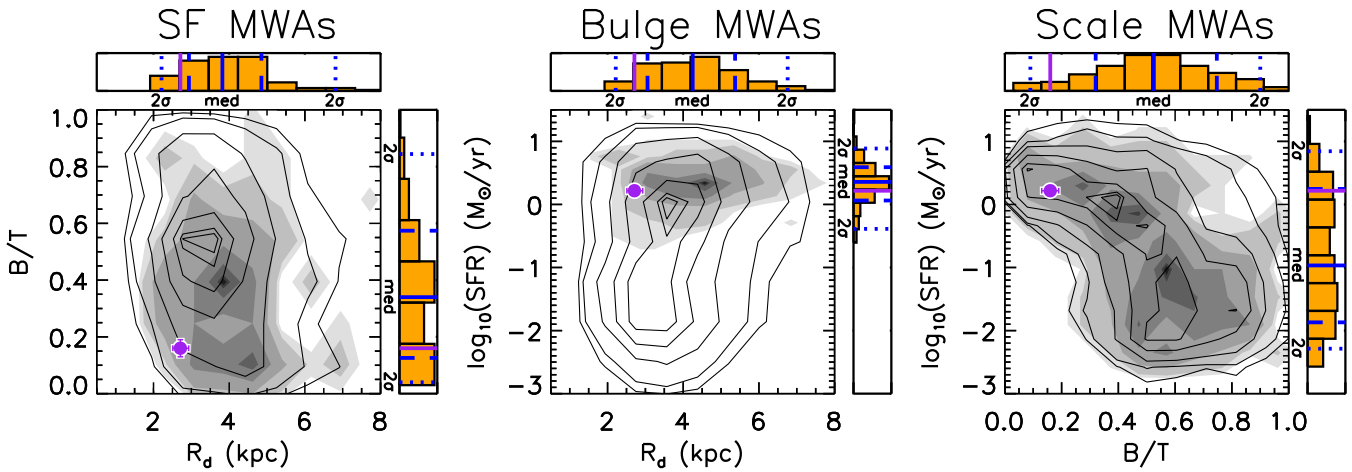

Figure 8. 2D and 1D histograms of parameter distributions for SF MWAs, bulge MWAs and scale MWAs, with the MW values shown in purple. The grey-scale surfaces represent the specific MWA samples, while the contours represent all galaxies that satisfy the MW mass cut. The contour levels represent 5 per cent, 10 per cent, 25 per cent, 50 per cent, 75 per cent, 90 per cent, and 95 per cent of the largest single bin. The blue solid lines represent the medians in a given parameter, the dashed lines the 1σ ranges, and the dotted lines the 2σ ranges.

adopted 10 per cent errors for the MW in line with previous work (e.g. Licquia et al. 2016); this leads to 1σ $V_{\rm rot}$ windows of 198–242 km s^{-1} and 197–255 km s^{-1} for the MW and M31, respectively, in turn. Due to the resulting overlap in the MW and M31 values, we selected a single analogue sample to cover $V_{\rm rot}$ values between 197 and 255 km s^{-1}; we restricted this selection to galaxies with inclinations no lower than 40^o and with velocity width errors no greater than 15 km s^{-1}. The resulting sample was found to be essentially complete, so we made no explicit redshift cut. We found the MW scale length to be offset low by over 1σ in this case, with our adopted central M31 SFR also low by roughly 1σ; both galaxies are otherwise in good consistency with this analogue sample. Our results from this sample are therefore similar to what we find with the other MWA and M31A samples. However, the use of H I data strongly biases the cross-matched parent sample towards disc-dominated star-forming galaxies, and we prefer our other analogue selections for this reason.

The difference in MWA and M31A results – particularly in terms of scale lengths – likely relate to the respective evolution histories of the MW and M31. Mackereth et al. (2018) report that bimodal alpha abundance ratios only appear in EAGLE galaxies when those galaxies have had a particularly violent early merging history, though other simulation works (e.g. Grand et al. 2018; Buck 2020) provide counterpoints. That the MW experienced an early merging history

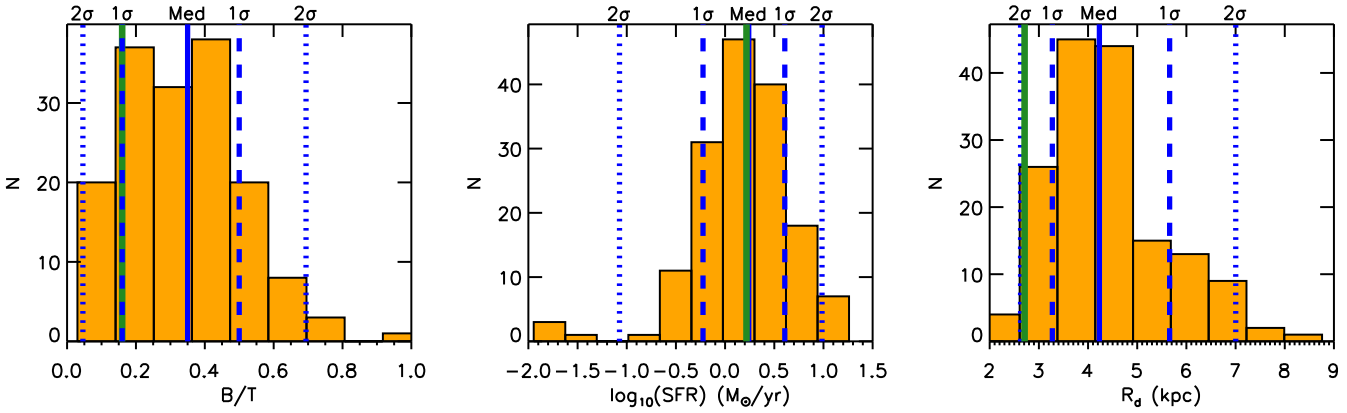

Figure 9. 1D histograms of parameter distributions for morphological MWAs. The blue solid lines show the medians of the MWA samples; the dashed blue lines indicate the 1σ regions, and the dotted blue lines indicate the 2σ regions. The central MW value is also shown in each window as a solid green line.

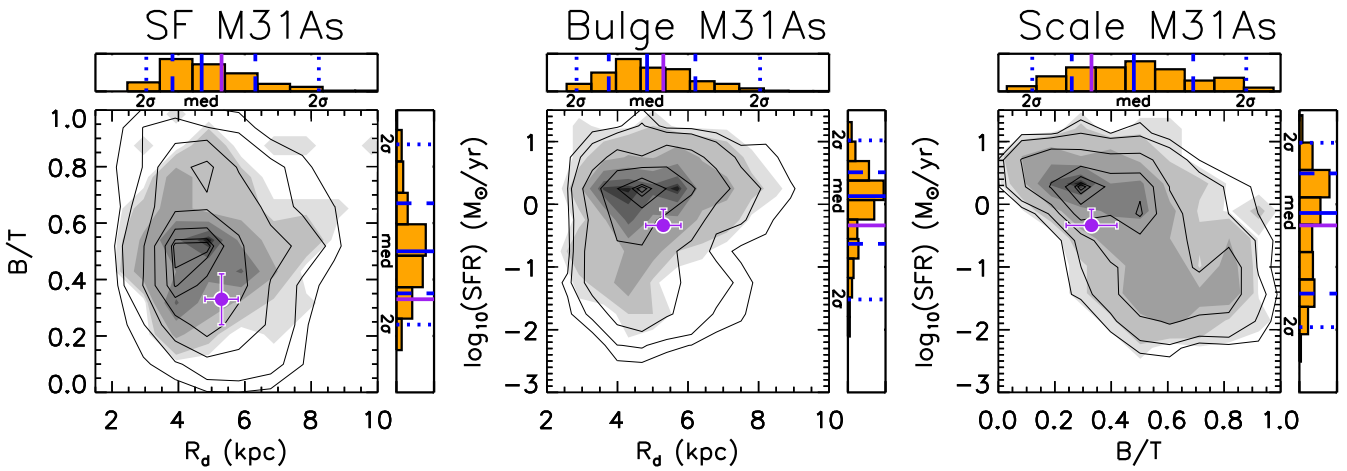

Figure 10. 2D and 1D histograms of parameter distributions for SF M31As, bulge M31As, and scale M31As, with the M31 values shown in purple. The grey scale surfaces represent the specific M31A samples, while the contours represent all galaxies that satisfy the M31 mass cut. The contour levels represent 5 per cent, 10 per cent, 25 per cent, 50 per cent, 75 per cent, 90 per cent, and 95 per cent of the largest single bin. The blue solid lines represent the medians in a given parameter, the dashed lines the 1σ ranges, and the dotted lines the 2σ ranges.

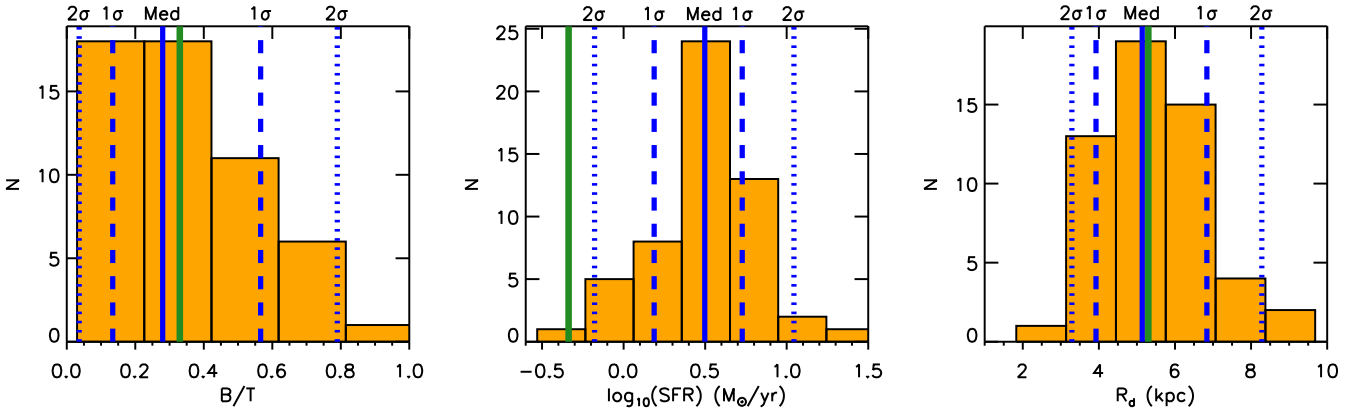

Figure 11. 1D histograms of parameter distributions for morphological M31As. The blue solid lines show the medians of the M31As; the dashed blue lines indicate the 1σ regions, and the dotted blue lines indicate the 2σ regions. The central M31 value is also shown in each window as a solid green line.

is supported by the age–metallicity distribution of MW globular clusters (Kruijssen et al. 2019) and by substructures apparent in *Gaia* data (Belokurov et al. 2018; Helmi et al. 2018; Elias et al. 2020), and the apparent short scale length of the MW can also be understood on this basis (Mo, Mao & White 1998). M31 likely had a more extended merging history, meanwhile, that is more typical of spiral galaxies (Hammer et al. 2007). Such a notion is consistent with the apparent burst in star formation that occurred in M31 roughly 2–4 Gyr ago

Table 3. Table of Milky Way Analogues, with no redshift cut applied. A flag value of '1' indicates a galaxy's status as a morphological MWA. We show the first five rows here; the full table will be made available online.

Objid (SDSS DR8)	RA (deg)	Dec. (deg)	z	$\log_{10}(M_*/M_\odot)$	$\log_{10}(\mathrm{SFR}/M_\odot\,\mathrm{yr}^{-1})$	B/T	R_d (kpc)	*Spiral*	*Bar*	Flag
1237663917872054658	111.586	43.533	0.057	10.75	− 2.21	0.40	2.75	0.00	0.00	0
1237663547431518682	111.638	37.914	0.082	10.79	− 1.48	0.49	2.88	1.00	0.98	0
1237663916797723168	111.981	41.959	0.058	10.81	0.18	0.41	4.36	0.61	0.93	0
1237663917335052608	112.048	42.981	0.066	10.76	0.41	0.81	4.02	0.97	1.00	1
1237663547432108541	112.500	39.100	0.089	10.84	0.23	0.17	6.05	0.09	0.98	0

Table 4. Table of Andromeda Analogues, with no redshift cut applied. A flag value of '1' indicates a galaxy's status as a morphological M31A. We show the first five rows here; the full table will be made available online.

Objid (SDSS DR8)	RA (deg)	Dec. (deg)	z	$\log_{10}(M_*/M_\odot)$	$\log_{10}(\mathrm{SFR}/M_\odot\,\mathrm{yr}^{-1})$	B/T	R_d (kpc)	*Spiral*	*Bar*	Flag
1237663917872185769	111.824	43.785	0.057	11.00	0.40	0.45	5.28	0.17	0.65	0
1237663916797985250	112.351	42.429	0.133	11.02	1.11	0.18	5.75	0.72	1.00	0
1237663530252238968	112.639	39.049	0.088	11.01	0.39	0.27	5.77	0.89	1.00	0
1237663787414782244	114.002	44.470	0.079	11.01	− 0.88	0.62	5.77	0.00	1.00	0
1237657594607501971	114.303	27.235	0.093	11.01	0.27	0.42	5.49	0.00	0.97	0

(Williams et al. 2015). This, along with the comparatively large amount of disc heating evident in M31 (Hammer et al. 2018) and the multiple substructures around M31 with similar stellar populations (Bernard et al. 2015), supports the idea of major merger occurring at around that time, with M32 being a possible remnant of the merging galaxy (D'Souza & Bell 2018).

Looking to larger galaxy samples, it has been reported that smaller galaxies display stellar populations that are on average older and more metal rich at a given galaxy mass (e.g. Scott et al. 2017; Li et al. 2018a). This is likewise consistent with the scenario of the MW having an atypical formation history amongst spiral galaxies, and further highlights the importance of considering disc scale length when setting out to select the most similar MWAs.

Given the apparent importance of scale length in understanding the MW, we further argue that scale length should be specifically considered when attempting to reproduce the MW in models and simulations, along with properties such as B/T and SFR. Simulation studies often focus on galaxies of MW-like mass (halo, stellar, or total), with environment also frequently taken into account (e.g. Scannapieco et al. 2015; Nuza et al. 2019; Carlesi et al. 2020; Santistevan et al. 2020). Additional selections can be imposed to ensure disc-domination in simulated galaxies identified as being MW-like, as for instance done in Mackereth et al. (2018), but such selections can still be expected to yield galaxies that are much more extended than the MW on average. By considering in simulations galaxies that match the MW in terms of a wider range of properties – in particular, by considering galaxies that are star-forming and disc-dominated while also possessing compact discs – the opportunity exists to further understand how our own Galaxy came to be.

To summarize, we find the MW's properties to mostly be in good consistency with its analogues, irrespective of the particular selection strategy employed. We do, however, find the MW disc to be atypically compact compared to the MWA samples, meaning that MWA samples do *not* accurately predict the MW's disc scale length unless the scale length is included in the selection criteria. We therefore argue that scale length should be considered *in addition* to other parameters when selecting the most stringent MWAs. We find M31's scale length to be in excellent agreement with its analogues, though its SFR is evidently lower than the majority of its structural peers. Thus, we advocate selecting on a combination of mass, SFR, and bulge fraction to choose the closest M31As.

ACKNOWLEDGEMENTS

We thank the anonymous referee for their comments, which served to greatly improve the clarity of this paper. We thank Cristina Chiappini for her useful and insightful comments on this manuscript.

The support and resources from the Center for High Performance Computing at the University of Utah are gratefully acknowledged.

DATA AVAILABILITY

The data underlying this article are available in its online supplementary material. We include as online supplementary material two tables detailing all MWAs and M31As, with no redshift cut applied. We show the first five rows of each of these tables in Tables 3 and 4.

REFERENCES

Abazajian K. N. et al., 2009, ApJS, 182, 543
Ahn C. P. et al., 2014, ApJS, 211, 17
Aihara H. et al., 2011, ApJS, 193, 29
Anders F. et al., 2014, A&A, 564, A115
Baldry I. K., Glazebrook K., Brinkmann J., Ivezić Ž., Lupton R. H., Nichol R. C., Szalay A. S., 2004, ApJ, 600, 681
Barbuy B., Chiappini C., Gerhard O., 2018, ARA&A, 56, 223
Barmby P. et al., 2006, ApJ, 650, L45
Beaton R. L. et al., 2007, ApJ, 658, L91
Belfiore F. et al., 2017, MNRAS, 466, 2570
Bell E. F. et al., 2004, ApJ, 608, 752
Belokurov V., Erkal D., Evans N. W., Koposov S. E., Deason A. J., 2018, MNRAS, 478, 611

Benjamin R. A. et al., 2005, ApJ, 630, L149
Bensby T., Feltzing S., Lundström I., 2003, A&A, 410, 527
Bernard E. J. et al., 2015, MNRAS, 446, 2789
Bland-Hawthorn J., Gerhard O., 2016, ARA&A, 54, 529
Blanton M. R., Kazin E., Muna D., Weaver B. A., Price-Whelan A., 2011, AJ, 142, 31
Blanton M. R. et al., 2017, AJ, 154, 28
Boardman N. et al., 2020, MNRAS, 491, 3672
Boquien M., Burgarella D., Roehlly Y., Buat V., Ciesla L., Corre D., Inoue A. K., Salas H., 2019, A&A, 622, A103
Bovy J., Rix H.-W., 2013, ApJ, 779, 115
Bovy J., Rix H.-W., Hogg D. W., 2012, ApJ, 751, 131
Buck T., 2020, MNRAS, 491, 5435
Buder S. et al., 2019, A&A, 624, A19
Bundy K. et al., 2015, ApJ, 798, 7
Cappellari M., 2016, ARA&A, 54, 597
Carignan C., Chemin L., Huchtmeier W. K., Lockman F. J., 2006, ApJ, 641, L109
Carlesi E., Hoffman Y., Gottlöber S., Libeskind N. I., Knebe A., Yepes G., Pilipenko S. V., 2020, MNRAS, 491, 1531
Chabrier G., 2003, PASP, 115, 763
Chang C.-K., Ko C.-M., Peng T.-H., 2011, ApJ, 740, 34
Chen B., Figueras F., Torra J., Jordi C., Luri X., Galadí-Enríquez D., 1999, A&A, 352, 459
Chiappini C., Matteucci F., Gratton R., 1997, ApJ, 477, 765
Chomiuk L., Povich M. S., 2011, AJ, 142, 197
Courteau S., Widrow L. M., McDonald M., Guhathakurta P., Gilbert K. M., Zhu Y., Beaton R. L., Majewski S. R., 2011, ApJ, 739, 20
Cui X.-Q. et al., 2012, Res. Astron. Astrophys., 12, 1197
D'Souza R., Bell E. F., 2018, Nat. Astron., 2, 737
De Silva G. M. et al., 2015, MNRAS, 449, 2604
Dékány I., Minniti D., Catelan M., Zoccali M., Saito R. K., Hempel M., Gonzalez O. A., 2013, ApJ, 776, L19
Deng L.-C. et al., 2012, Res. Astron. Astrophys., 12, 735
Dwek E. et al., 1995, ApJ, 445, 716
Elbaz D. et al., 2007, A&A, 468, 33
Elias L. M., Sales L. V., Helmi A., Hernquist L., 2020, MNRAS, 495, 29
Faber S. M. et al., 2007, ApJ, 665, 265
Fathi K., Allen M., Boch T., Hatziminaoglou E., Peletier R. F., 2010, MNRAS, 406, 1595
Fraser-McKelvie A., Merrifield M., Aragón-Salamanca A., 2019, MNRAS, 489, 5030
Fuhrmann K., 1998, A&A, 338, 161
Fuhrmann K., 2011, MNRAS, 414, 2893
Geehan J. J., Fardal M. A., Babul A., Guhathakurta P., 2006, MNRAS, 366, 996
Gilmore G., Reid N., 1983, MNRAS, 202, 1025
Gilmore G. et al., 2012, The Messenger, 147, 25
Grady J., Belokurov V., Evans N. W., 2020, MNRAS, 492, 3128
Grand R. J. J. et al., 2018, MNRAS, 474, 3629
Hammer F., Puech M., Chemin L., Flores H., Lehnert M. D., 2007, ApJ, 662, 322
Hammer F., Yang Y. B., Wang J. L., Ibata R., Flores H., Puech M., 2018, MNRAS, 475, 2754
Hammersley P. L., Garzon F., Mahoney T., Calbet X., 1994, MNRAS, 269, 753
Hart R. E. et al., 2016, MNRAS, 461, 3663
Hart R. E., Bamford S. P., Casteels K. R. V., Kruk S. J., Lintott C. J., Masters K. L., 2017, MNRAS, 468, 1850
Hayden M. R. et al., 2015, ApJ, 808, 132
Haynes M. P. et al., 2018, ApJ, 861, 49
Haywood M., Di Matteo P., Lehnert M. D., Katz D., Gómez A., 2013, A&A, 560, A109
Helmi A., Babusiaux C., Koppelman H. H., Massari D., Veljanoski J., Brown A. G. A., 2018, Nature, 563, 85
Hughes T. M. et al., 2014, A&A, 565, A4
Kang Y., Bianchi L., Rey S.-C., 2009, ApJ, 703, 614
Kent S. M., 1992, ApJ, 387, 181
Kent S. M., Dame T. M., Fazio G., 1991, ApJ, 378, 131
Kerr F. J., Lynden-Bell D., 1986, MNRAS, 221, 1023
Kormendy J., Bender R., 2019, ApJ, 872, 106
Krishnarao D. et al., 2020, ApJ, 898, 116
Kroupa P., 2001, MNRAS, 322, 231
Kruijssen J. M. D., Pfeffer J. L., Reina-Campos M., Crain R. A., Bastian N., 2019, MNRAS, 486, 3180
Kruk S. J. et al., 2018, MNRAS, 473, 4731
Laurikainen E., Salo H., Buta R., 2005, MNRAS, 362, 1319
Laurikainen E., Salo H., Buta R., Knapen J., Speltincx T., Block D., 2006, AJ, 132, 2634
Li H. et al., 2018a, MNRAS, 476, 1765
Li C., Zhao G., Zhai M., Jia Y., 2018b, ApJ, 860, 53
Licquia T. C., Newman J. A., 2015, ApJ, 806, 96 (LN15)
Licquia T. C., Newman J. A., 2016, ApJ, 831, 71 (LN16)
Licquia T. C., Newman J. A., Brinchmann J., 2015, ApJ, 809, 96
Licquia T. C., Newman J. A., Bershady M. A., 2016, ApJ, 833, 220
Mackereth J. T. et al., 2017, MNRAS, 471, 3057
Mackereth J. T., Crain R. A., Schiavon R. P., Schaye J., Theuns T., Schaller M., 2018, MNRAS, 477, 5072
Majewski S. R. et al., 2017, AJ, 154, 94
Mao Q. et al., 2015, preprint (arXiv:1507.01593)
Martig M., Minchev I., Ness M., Fouesneau M., Rix H.-W., 2016, ApJ, 831, 139
Martin D. C. et al., 2005, ApJ, 619, L1
McWilliam A., Zoccali M., 2010, ApJ, 724, 1491
Mikolaitis Š et al., 2014, A&A, 572, A33
Minchev I., Martig M., Streich D., Scannapieco C., de Jong R. S., Steinmetz M., 2015, ApJ, 804, L9
Mo H. J., Mao S., White S. D. M., 1998, MNRAS, 295, 319
Mocz P., Green A., Malacari M., Glazebrook K., 2012, MNRAS, 425, 296
Mouhcine M., Ibata R., Rejkuba M., 2010, ApJ, 714, L12
Mutch S. J., Croton D. J., Poole G. B., 2011, ApJ, 736, 84
Nidever D. L. et al., 2014, ApJ, 796, 38
Noll S., Burgarella D., Giovannoli E., Buat V., Marcillac D., Muñoz-Mateos J. C., 2009, A&A, 507, 1793
Nuza S. E., Scannapieco C., Chiappini C., Junqueira T. C., Minchev I., Martig M., 2019, MNRAS, 482, 3089
Queiroz A. B. A. et al., 2019, A&A , 638, A76
Recio-Blanco A. et al., 2014, A&A, 567, A5
Rojas-Arriagada A., Zoccali M., Schultheis M., Recio-Blanco A., Zasowski G., Minniti D., Jönsson H., Cohen R. E., 2019, A&A, 626, A16
Ruelas-Mayorga R. A., 1991, Rev. Mex. Astron. Astrofis., 22, 27
Saha K., Cortesi A., 2018, ApJ, 862, L12
Salim S. et al., 2007, ApJS, 173, 267
Salim S. et al., 2016, ApJS, 227, 2
Salim S., Boquien M., Lee J. C., 2018, ApJ, 859, 11
Sandage A., Tammann G. A., 1981, A Revised Shapley-Ames Catalogue of Bright Galaxies, Carnegie Institution of Washington, Washington, D.C.
Santistevan I. B., Wetzel A., El-Badry K., Bland-Hawthorn J., Boylan-Kolchin M., Bailin J., Faucher-Giguère C.-A., Benincasa S., 2020, MNRAS, 497, 747
Scannapieco C., Creasey P., Nuza S. E., Yepes G., Gottlöber S., Steinmetz M., 2015, A&A, 577, A3
Schawinski K. et al., 2014, MNRAS, 440, 889
Schlafly E. F., Finkbeiner D. P., 2011, ApJ, 737, 103
Schlegel D. J., Finkbeiner D. P., Davis M., 1998, ApJ, 500, 525
Scott N. et al., 2017, MNRAS, 472, 2833
Simard L., Mendel J. T., Patton D. R., Ellison S. L., McConnachie A. W., 2011, ApJS, 196, 11
Smethurst R. J. et al., 2015, MNRAS, 450, 435
Steinmetz M. et al., 2006, AJ, 132, 1645
Strateva I. et al., 2001, AJ, 122, 1861
Tamm A., Tempel E., Tenjes P., Tihhonova O., Tuvikene T., 2012, A&A, 546, A4
Tully R. B., Fisher J. R., 1977, A&A, 54, 661

Wegg C., Gerhard O., 2013, MNRAS, 435, 1874
Weiland J. L. et al., 1994, ApJ, 425, L81
Widrow L. M., Pym B., Dubinski J., 2008, ApJ, 679, 1239
Willett K. W. et al., 2013, MNRAS, 435, 2835
Williams B. F. et al., 2015, ApJ, 806, 48
Willick J. A., Courteau S., Faber S. M., Burstein D., Dekel A., Strauss M. A., 1997, ApJS, 109, 333
Wright E. L. et al., 2010, AJ, 140, 1868
Wu Y. et al., 2019, MNRAS, 484, 5315
Wu P.-F., 2018, MNRAS, 473, 5468
Xiang M. et al., 2017, ApJS, 232, 2
Yamagata T., Yoshii Y., 1992, AJ, 103, 117
Yin J., Hou J. L., Prantzos N., Boissier S., Chang R. X., Shen S. Y., Zhang B., 2009, A&A, 505, 497
York D. G. et al., 2000, AJ, 120, 1579
Yoshii Y., 1982, PASJ, 34, 365
Yoshino A., Yamauchi C., 2015, MNRAS, 446, 3749
Zahid H. J., Dima G. I., Kewley L. J., Erb D. K., Davé R., 2012, ApJ, 757, 54

SUPPORTING INFORMATION

Supplementary data are available at *MNRAS* online.

Table 3. Table of Milky Way Analogues, with no redshift cut applied.
Table 4. Table of Andromeda Analogues, with no redshift cut applied.

Please note: Oxford University Press is not responsible for the content or functionality of any supporting materials supplied by the authors. Any queries (other than missing material) should be directed to the corresponding author for the article.

This paper has been typeset from a TEX/LATEX file prepared by the author.